 FDMP, vol.5, no.3, pp.211-230, 2009

Three Dimensional Modeling of $Ge_{0.98}$ $Si_{0.02}$ Crystal Growth Conducted on board FOTON-M2 in the Presence of Rotating Magnetic Field

M.M. Shemirani[1] **and M.Z. Saghir**[2]

Abstract: A three-dimensional numerical modeling of $Ge_{0.98}$ $Si_{0.02}$crystal growth is conducted to investigate the effect of g-jitter along with rotating magnetic field on the heat and mass transfer in the solvent region. It was found that the speed in the flow under the low frequency g-jitter is in the nano-centimeter per second and is too weak to have any impact on the silicon concentration in the process of crystallization near the growth interface. Different magnetic field intensities for different rotational speeds were examined. It was also found that rotating magnetic field not only did not suppress the convection but also generated an undesirable convective motion in the solvent region which is unsuitable for achieving the uniform and homogeneous crystal growth near the growth interface.

Keywords: Crystal growth, G-jitter, TSM, RMF, Micro-gravity, FOTON-M2

Nomenclature

(Dimensionless variables are detailed in Appendix C)

B_1	Magnetic field Induction, "r" direction (Tesla)
B_2	Magnetic field Induction, "φ" direction (Tesla)
C	Dimensionless concentration
C	Solute concentration (atomic %)
C_o	Reference solute concentration (atomic %)
L	Reference length (volume /surface area)
r	Radial direction (cm)
R	Dimensionless radial coordinate
T_o	Reference Temperature (°C)
U	Dimensionless Velocity in "r" direction

[1] Ryerson University, Toronto, ON, M5B 2K3, Canada
[2] Corresponding Author, Ryerson University, Toronto, ON M5B 2K3, Canada

V Dimensionless Velocity in "φ" direction
W Dimensionless Velocity in "Z" direction
z Axial direction (cm)
Z Dimensionless axial coordinate
α_c Solutal (mass) diffusivity of the specie (cm^2/s)
β_c Solutal expansion coefficient (1/at % Si)
β_T Thermal expansion coefficient (1/°C)
φ Circumferential direction
τ Dimensionless Time
θ Dimensionless temperature
Ω Rotational speed (rpm)
ω^* Dimensionless Angular Velocity

Subscript

o Reference
m Melt

Superscript

M Magnetic Field

1 Introduction

In today's world with the rapid increase in demand for electronic devices which incorporate semiconductors, it is obvious to expect a perfect and flawless product such as computers, life saving medical devices, game consoles, cellular phones, graphic displays, and digital audio and video players to name a few IUPAC (1982). The reliability of the aforementioned products is highly dependent on the performance of the semiconductors being used in them. This reliance is based on the consistency of the internal arrangement of atoms in a three dimensional crystal structure and characteristics such as uniformity and purity of a bulk single crystal. The authors of this paper have shown in their previous studies how to suppress the buoyancy induced convection which is an undesirable effect in the process of bulk single crystal growth in terrestrial condition by applying rotating magnetic field (RMF).

In this paper we are attempting to investigate the effects of residual acceleration or g-jitter on the fluid flow in the solvent region by solving numerically the full Navier Stokes equations combined with the energy and mass transfer equations using the finite element technique. The term g-jitter, also known as residual acceleration, means that the experiment which will be conducted in the space environment

is subjected to low frequency disturbances generated randomly on board FOTON platform. Disturbances could be generated from an astronaut moving, fans, running an experiment with different motorized equipments, orbiter positioning rocket etc. Lehoczky, Szofran and Gillies (1994). Muller and Baumgartl (1996) utilized a magnetic field to damp the action of gravity fluctuations (g-jitter) during crystal growth under microgravity. It was shown that melt flow oscillations caused by residual accelerations (g-jitter) in crystal growth experiments under microgravity, can effectively be reduced by static magnetic fields. The reduction of the amplitudes of the flow oscillations is depending on the excitation frequency. Strength and orientation of the magnetic field ($\sim$ 50 mT) are found to be important parameters. It was also stated that Since the (Prandtl number) Pr «1 for metal or semiconductor melts, the influence of g-jitter flows on the temperature field can be neglected for practical purposes, on the contrary the effect on solutal fields (Schmidt number) Sc»1 can be very noticeable. Thus g-jitter can cause the formation of compositional fluctuations (striations). The flow amplitude induced by Δg_{01} are of order of 1 nm/s and are thus sufficiently small not to be harmful to a growing crystal, whereas higher g-jitter amplitude like Δg_{100} can result in flow fluctuations that can provide an additional transport mechanism for solute species which is in general undesirable under micro-gravity (mg) conditions. Li (1996) conducted an analytical analysis on g-jitter induced flow in the microgravity under the influence of a transverse magnetic field. It was shown that the g-jitter frequency, applied magnetic field and temperature gradients all contribute to affect convective flow. Also it was found that amplitude of velocity decreases at a rate inversely proportional to the g-jitter frequency. Magnetic field can suppress the oscillating flows associated with the g-jitter and act as a damper. It is more effective for low frequency oscillation and has moderate effect on high frequency oscillation as a result of g-jitter. Temperature gradient has a profound effect on the g-jitter induced flow. A residual gravity of 10^{-5} and 10^{-6} is found to be sufficient to cause unacceptable fluid motion in the liquid. For a time harmonic g-jitter with a frequency w, $g(t)=g_0e^{jwt}$, the flow field and the induced electric field should have a similar time varying behavior. Yeckel and Derby (2004) studied the transient accelerations in both axial and transverse directions in a simple prototype of a vertical Bridgman crystal growth technique. The residual acceleration was set to 10^{-6} and the jitter amplitude to 10^{-4} (used in US space shuttle). The effect of jitter on flow response over a wide range of frequencies and magnetic field has been studied. The effect of a steady magnetic field is to suppress flow in the low-frequency regime. For the conditions studied here, a transverse jitter of 10 Hz had essentially no impact on the flow, where as jitter below 10^{-3} Hz induced a quasi-steady (semi-steady) flow response. It was also stated that while a typical growth experiment occurs in hours scale, the g-jitter occurs on sub-second scale. Axial magnetic field has more and stronger effect on reducing

axial flow regardless of the expected g-jitter pattern. It was noted that rather than simply attempting to suppress flow altogether, the ability to selectively filter one of the flow components suggests an alternate approach to manipulating mass convection. Yasuda, Minakuchi, Okano and Dost (2004) on their study on g-jitter induced melt convection found that the g-jitter in the vertical direction to the temperature gradient was more enhanced than the parallel direction when magnetic field (Ha = 50) and frequency was 0.01Hz on the flow field.

2 Model Description

The model consists of a fixed cylindrical coordinate system of (r, ϕ, z) with its origin located at the center of the growth interface. The original model is 6.1 cm long with a uniform diameter of 0.8 cm and consists of three segments as; seed (Germanium) 1.5 cm, the solvent region 1cm which is a mixture of silicon (Si) and germanium (Ge) initially set as $Ge_{0.98}$ $Si_{0.02}$, which is the middle segment and source ($Ge_{0.85}Si_{0.15}$) 3.1 cm. the traveling solvent method (TSM) is the technique being chosen for this study. All three sections, introduced earlier in model description, are held in a quartz ampoule; Labrie, George, Jamieson, Obruchkov, Healey, Paton and Saghir (2005). Since the melt temperature of the solvent region is much less than that of the quartz, therefore there would be no oxygen penetration from quartz into the melt and consequently no contamination or impurity occurs which is a great advantage of this technique. Figure 1, depicts the solvent region of the (TSM) under this study.

3 Boundary Condition

In this model, an equilibrium boundary condition on mass balance is used on the growth interface. The boundary conditions are as follow:

a) At the ampoule side wall (solid);

$$u = 0, \quad v = 0 \text{ and } w = 0 \text{ (Non-slip condition) and } \frac{\partial c}{\partial r} = 0$$

b) At the dissolution interface which is on the top horizontal plane;

$$c = c_1 = 0.15$$

c) At the growth interface which is on the bottom horizontal plane;

$$c = c_2 = 0.02$$

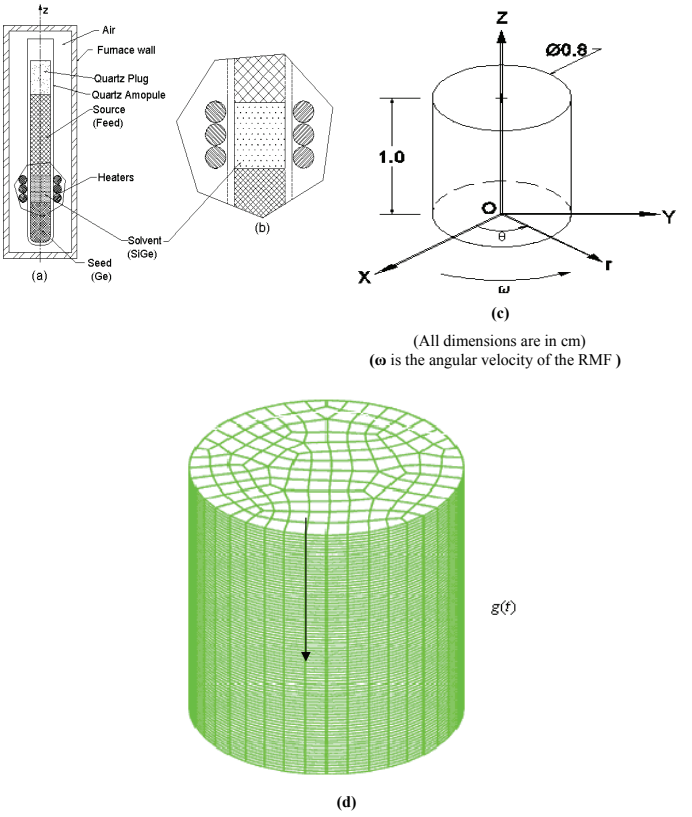

Figure 1: Solvent region under investigation; a) Schematic of TSM Furnace; b) Solvent Region under this study; c) Coordinates of the Model; d) Meshed Model

Where c_1 and c_2 are representing the silicon concentration in the crystal growth process. At the external surface of the quartz ampoule (not shown in the Figure 1) a non uniform temperature distribution is applied uniformly in the radial direction. This temperature profile which is unsymmetrical in the azimuthal direction was measured experimentally at Dalhousie University. Appendix "A" detailed the temperature boundary condition.

The main physical properties of the solvent which are taken into the consideration are incorporated in the Table 1.

4 Governing Equations

Navier-Stokes Equations: The Laminar Newtonian Fluid's motion is governed by the Navier-Stokes equations and would be described and solved for each axis

Table 1: Properties of GeSi

Physical Properties of $Ge_{0.98}$ $Si_{0.02}$	
Symbol	**Values Units**
c_p	0.04008 J/g.K
T_m	971 °C
α_c	0.52×10^{-4} cm^2/s
σ	2.5×10^{4}S/cm
β_c	0.0051 / at% Si
β_T	1.01×10^{-4} 1/°C
κ	0.2559 W/cm/K
μ	8.3496×10^{-3}g/cm.s
ν	1.53192×10^{-3}cm^2 /s
ρ	5.4504 g/cm^3

of the cylindrical coordinate system in unsteady state (Transient) by taking Boussinesq approximation into the consideration. In the non-dimensional forms the governing equations are as follow:

r-component:

$$Re\left(\frac{\partial U}{\partial \tau}+U\frac{\partial U}{\partial R}+\frac{V}{R}\frac{\partial U}{\partial \varphi}+W\frac{\partial U}{\partial Z}-\frac{V^2}{R}\right)=$$
$$-\frac{\partial P}{\partial R}+\left(\frac{\partial^2 U}{\partial R^2}+\frac{1}{R^2}\frac{\partial^2 U}{\partial \varphi^2}+\frac{\partial^2 U}{\partial Z^2}-\frac{U}{R^2}-\frac{2}{R^2}\frac{\partial V}{\partial \varphi}\right)$$
$$-\frac{1}{2}Ha^2\omega^* B_1^2+\frac{(Gr_T)_r}{Re}\theta-\frac{(Gr_C)_r}{Re}C \quad (1)$$

ϕ-component:

$$Re\left(\frac{\partial V}{\partial \tau}+U\frac{\partial V}{\partial R}+\frac{V}{R}\frac{\partial V}{\partial \varphi}+W\frac{\partial V}{\partial Z}+\frac{UV}{R}\right)=$$
$$-\frac{1}{R}\frac{\partial P}{\partial \varphi}+\left(\frac{\partial^2 V}{\partial R^2}+\frac{1}{R^2}\frac{\partial^2 V}{\partial \varphi^2}+\frac{\partial^2 V}{\partial Z^2}-\frac{V}{R^2}+\frac{2}{R^2}\frac{\partial V}{\partial \varphi}\right)$$
$$+\frac{1}{2}Ha^2\omega^* B_2^2+\frac{(Gr_T)_\varphi}{Re}\theta-\frac{(Gr_C)_\varphi}{Re}C \quad (2)$$

z-component:

$$Re\left(\frac{\partial W}{\partial \tau}+U\frac{\partial W}{\partial R}+\frac{V}{R}\frac{\partial W}{\partial \varphi}+W\frac{\partial W}{\partial Z}\right)= \\ -\frac{\partial P}{\partial Z}+\left(\frac{\partial^2 W}{\partial R^2}+\frac{1}{R^2}\frac{\partial^2 W}{\partial \varphi^2}+\frac{\partial^2 W}{\partial Z^2}\right)+\frac{(Gr_T)_Z}{Re}\theta-\frac{(Gr_C)_Z}{Re}C \quad (3)$$

The above equations (1-3) satisfy the momentum equations in the solvent region in the radial (r), angular (ϕ) and axial (z) directions by taking the Boussinesq approximation into the consideration. Where (Re) is the Reynolds number and Hartman number (Ha) is the non-dimensional form of the magnetic field effect. In the above equations Gr_T is the thermal Grashof number and Gr_C is the solutal Grashof number. In the r and ϕ components of the momentum equations, the term $\frac{1}{2}Ha^2\omega^* B_i^2$ is reflecting the assumption made by Gelfgat (1995) and Ghaddar (1999) for the magnetic body forces and it should be noted that magnetic force has no effect on the z axis based on their assumption. It is important to mention that in this analysis the electrical field is neglected for the sake of the simplicity of the model.

Energy Equation: which is defined for the solvent region's as follow:

$$\left(\frac{\partial \theta}{\partial \tau}+U\frac{\partial \theta}{\partial R}+\frac{V}{R}\frac{\partial \theta}{\partial \varphi}+W\frac{\partial \theta}{\partial Z}\right)=\frac{1}{Re.\,\mathrm{Pr}}\left(\frac{\partial^2 \theta}{\partial R^2}+\frac{1}{R^2}\frac{\partial^2 \theta}{\partial \varphi^2}+\frac{\partial^2 \theta}{\partial Z^2}\right) \quad (4)$$

Where (Pr) is the Prandtl *number.*

Continuity equation: Solvent's continuity equation reads as:

$$\left(\frac{\partial \rho}{\partial \tau}+\frac{1}{R}\frac{\partial}{\partial R}(RU)+\frac{1}{R}\frac{\partial V}{\partial \varphi}+\frac{\partial W}{\partial Z}\right)=0 \quad (5)$$

Solute equation: The mass transfer is governed by the following equation:

$$\left(\frac{\partial C}{\partial \tau}+U\frac{\partial C}{\partial R}+\frac{V}{R}\frac{\partial C}{\partial \varphi}+\frac{\partial W}{\partial Z}\right)=\frac{1}{Re.Sc}\left(\frac{\partial^2}{\partial R^2}+\frac{1}{R^2}\frac{\partial^2 C}{\partial \varphi^2}+\frac{\partial^2 C}{\partial Z^2}\right) \quad (6)$$

Where the solutal diffusion coefficient is represented by dimensionless Schmidt (Sc) number.

5 Mesh Sensitivity and Solution Technique

In order to have the best and most reliable results, an optimum number of nodes and elements should be defined, therefore, mesh sensitivity analysis was carried out and ideal numbers of nodes on both circumferential and axial edges were selected based on the heat flux across the dissolution interface in solvent region. As it can be read from the Figure 2, a mesh with 40 circumferential nodes by 80 axial nodes is where heat flux does not change and the mesh becomes finer. For this reason and the aforementioned reasons, the 40 x 80 mesh combination reasonably meets the computational need and simulation becomes satisfactory for the analysis in this study.

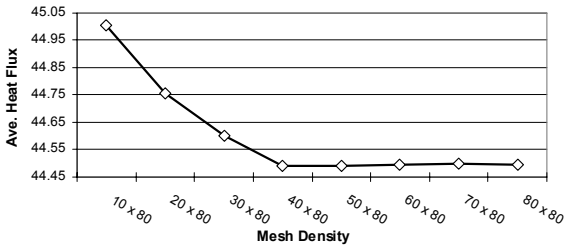

Figure 2: Mesh density vs. heat flux at dissolution interface

Finite element method is utilized and the model is divided into elements and subsequently nodes by which all the variables, which are the three velocities, concentration, pressure and the temperature can be evaluated and analyzed. In this model, which has over fourteen thousands nodes, the Galarkin finite element method approximation has been employed for silicon concentration and velocity in the solvent region along three axes (u, v, w). The governing equations then solved simultaneously and criteria for the convergence considered for the aforementioned variables. For convergence checking between two successive time steps the following equations are set to be met; $\frac{\|\Delta u_i\|}{\|u\|} \leq \varepsilon_u$, $\Delta u_i = u_i - u_{i-1}$ and $\frac{\|R_i\|}{\|R_0\|} \leq \varepsilon_F$ are used where "u_i" represents the pressure, temperature, velocities and silicon concentration, along "r, ϕ and z" directions for each node and "R_0" is reference vector, typically $R(u_i)$ which is the residual force vector. ε_u is the convergence tolerance based on the relative error and ε_F is the residual convergence tolerance for each variable at each iteration. Since both Δu_i and $R(u_i)$ tend to zero near the solution therefore problem is assumed converged when system satisfies the above criteria which was specified as 10^{-4} for both solution vector and residual force vector. For our study the maximum number of nonlinear iterations for both fluid and structural problem is set to

250. The norm |||| is a root mean square norm summed over all the equations for the model.

6 Results and Discussion

6.1 Growth of SiGe in terrestrial and microgravity condition

6.1.1 Terrestrial Condition

Figure 3, shows both a vertical cross section view (a) of the solvent region passing through the "z" axis of the model and a horizontal cross section plane (b) at z=0.1 cm above growth interface which reveals the concentration of Si in the solvent region in the terrestrial condition. It is clear that there is no homogeneity in the silicon distribution in the vertical plane passing through the "z" axis of the model due to buoyancy convection. Where as Figure 4 illustrates, the silicon concentration contours are more uniformly paralleled and clearly the convective motion in the solvent region has been suppressed, in (a) which is a vertical cross section along "z" axis and more co-centric in (b) which is a horizontal cut plane at 1mm above the growth interface and in terms of the percentage of concentration is very close to the targeted value which is 2 percent and it is ranged from 2.3 percent near the crucible wall to 3.4 percent at the center. It should be noted that authors have shown in their previous work the variety of intensities of the applied rotating magnetic filed and it was found that the combination of the 15mT magnetic intensity and 2 revolutions per minute would lead in a comparable results to those of the microgravity condition. It is, however, noticeable that there is slight concave into the solvent at the interface which in spite of stress built up in it, is on the other hand beneficial for growth process (i.e dewetting).

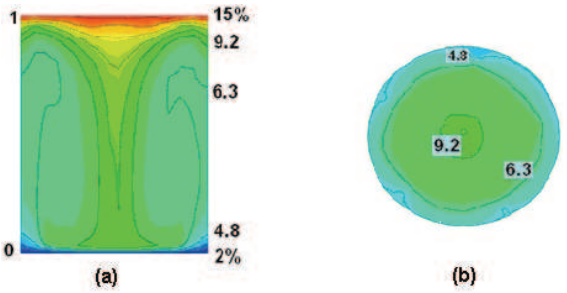

Figure 3: Silicon concentration contours, Terrestrial, with no rotating magnetic field; a) Vertical cross section along "z" axis of the model; b) Horizontal cross section at z=0.1cm above; growth interface

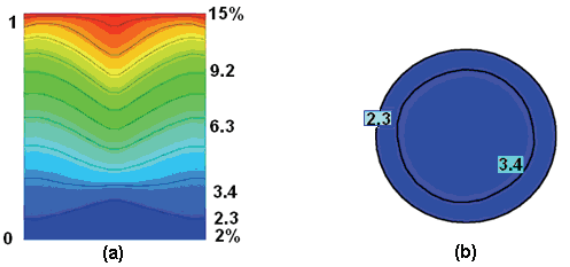

Figure 4: Silicon concentration contours, terrestrial condition with B = 15mT & Ω= 2 rpm; a) Vertical cross section along "z" axis of the model; b) Horizontal cross section at z=0.1cm above; growth interface

6.1.2 Microgravity Condition

Microgravity condition is referred to when magnitude of the gravity is in the range of $g = g_0 \times 10^{-4}$ to $g = g_0 \times 10^{-6}$ Figure 5 illustrates the silicon concentration where the contours are uniform and parallel to the growth interface.

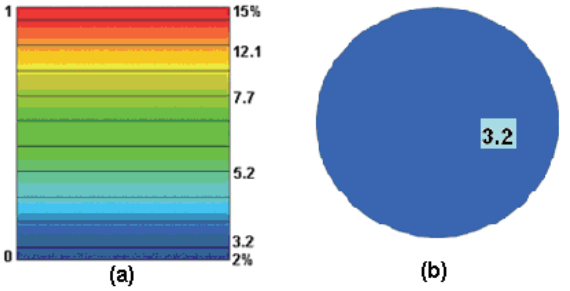

Figure 5: Silicon concentration contours in microgravity; a) Vertical cross section along "z" axis; b) Horizontal cross section at z=0.1cm

6.2 Effects of g-jitter on fluid flow

The intention is to examine if the residual accelerations can cause any convection in the melt region during the growth process. For this purpose, we investigated the effects of g-jitter on fluid flow with and without the presence of rotating magnetic field.

6.2.1 Evaluating the gravity "g" magnitude

The gravity for the last term in the momentum equations (r and ϕ components) which is embedded in Grashof number (Gr) both thermal $Gr_T = \frac{\beta_T \Delta T L^3 g \rho^2}{\mu^2}$ and solutal $Gr_c = \frac{\beta_T \Delta C L^3 g \rho^2}{\mu^2}$, consists of two components when g-jitter effects are to be studied; they are static and vibration which their dimensional format are defined as follow:

$$g = g_{st} + g_{vib} \tag{7}$$

This would be applied for all three axes. Where,

$$g_{st} = a_i^0 \tag{8}$$

$$g_{vib} = \sum a_i^1 \sin(2\pi f_i t) + b_i^1 \cos(2\pi f_i t) \tag{9}$$

Data collected, (see appendix B), from the FOTON-M2 in a tabulated format by Yan, Pan and Saghir (2007) were utilized in the equations 7-9 and results used in the simulation of the model under this study. Figure 6 represents the gravity oscillations over three different axes within the first 3600 second of the process in which it is found that the "Y" direction has the shortest time interval equal to 520 seconds and can be used as the base for the calculation and simulations. This is clearly indicated in Figure 3b where the amplitude is much larger than in the X and Z direction.

6.2.2 No Rotating Magnetic Field

Figure 7 shows the speed contour plots in radial, circumferential and axial directions, where the reference speed is defined by $u_0 = \sqrt{g\beta_T \Delta T L}$ (see appendix "C" for the definition of the non dimensionalized variables) and its magnitude in microgravity condition is u_0 = 0.009954 cm/s. By taking this multiplier into the consideration to interpret the legends in this figure, it is revealed that the speed varies between as low as 4.24×10^{-10}cm/s to as high as 1.05×10^{-9} cm/s. This speed is too weak to have any impact on the silicon concentration distribution.

It was also noted since the Prandtl number (Pr=1.3×10^{-3}) is much less than 1, the g-jitter effects on the temperature, Figure 8, can be neglected for practical purposes. As noticed in Figure 8, the temperature distribution is assymetrical since the applied temperature is non uniform in the azimuthal direction. Since crystal growth with TSM process is very slow, at a rate of 4mm per day, the 14 hours observation of the process reveals the flow behavior. Figure 9 shows the velocity plots under the influence of g-jitter which indicates the fluctuations become stable after about 14400 seconds.

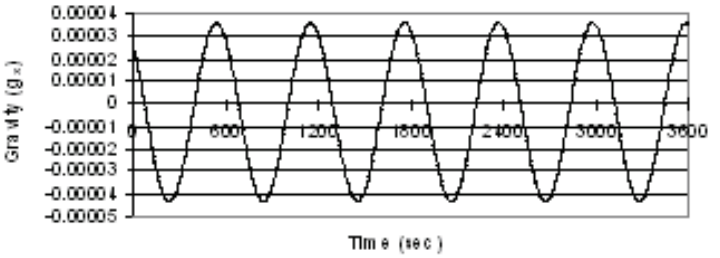

(a) In "X" direction with $\Delta t = 600$ sec

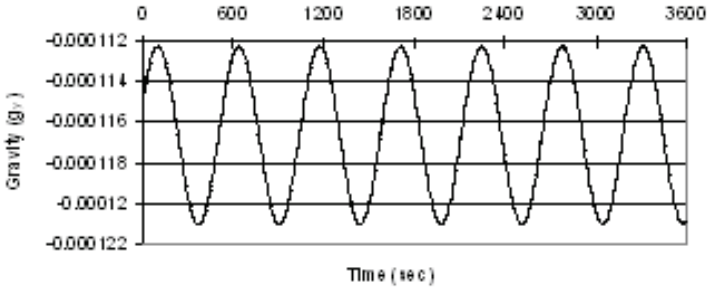

(b) In "Y" direction with $\Delta t = 520$ sec

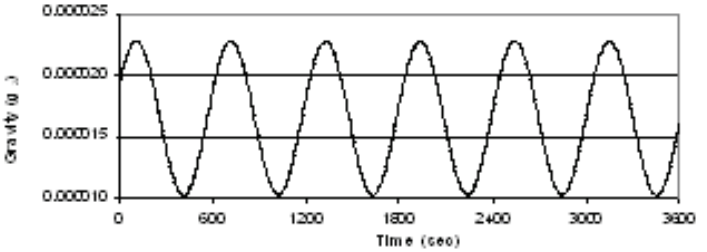

(c) In "Z" direction with $\Delta t = 608$ sec

Figure 6: Plots of g-jitter magnitude in 3 different directions

Again, these sets of plots reveal that the speed fluctuations are in nano centimeter per second in all the directions. Since the Schmidt number (Sc=29) is larger than 1, the effect of g-jitter on the solutal field should be investigated. Figure 10 which is a cross section of the model along "Z" axis shows that this low speed has no impact on the silicon distribution and contours are remained uniform and parallel to the growth interface as it is the desirable configuration.

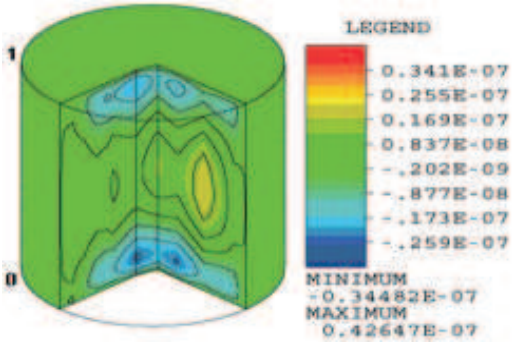

(a) In Radial direction

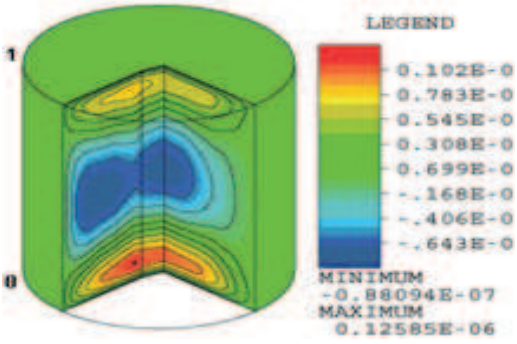

(b) In Circumferential direction

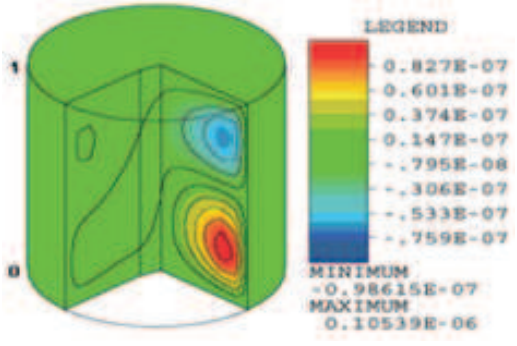

(c) In Axial direction

Figure 7: Speed contour Plots under g-jitter effect

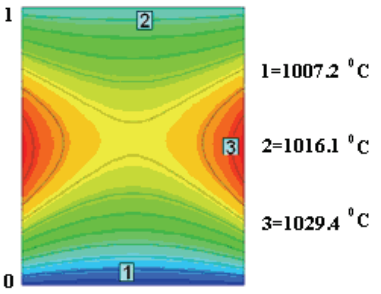

Figure 8: Temperature distribution contours; (a) Radial direction; (b) Circumferential direction; (c) Axial direction

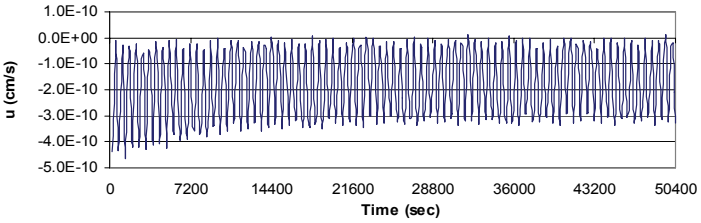

(a) Radial direction

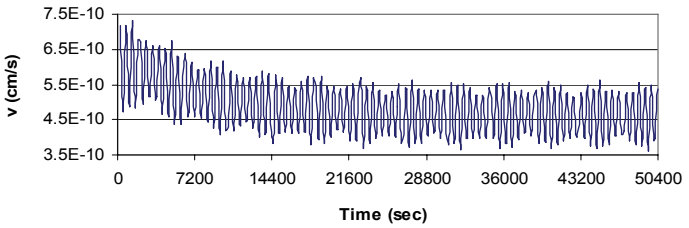

(b) Circumferential direction

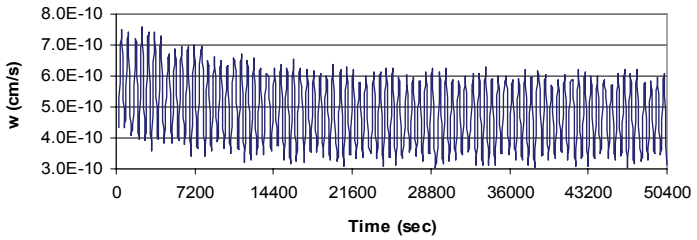

(c) Axial direction

Figure 9: Velocity Plots under the effect of g-jitter for the first 14 hours of the process

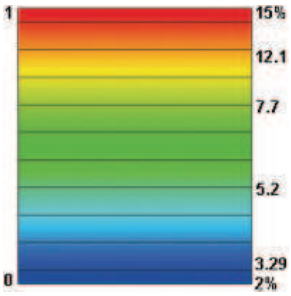

Figure 10: Silicon distribution contour in vertical cross section passing through the centre of the interface of the model

6.2.3 Applied 15mT Magnetic Force with 1/12 rpm

In order for us to investigate the flow behavior and to see whether we can enhance the flow and have it convection free or not, the presence of the magnetic field is studied. We have applied different magnetic field (B) intensities ((from 1 to 20 mili-Tesla (mT)) and found that the B=15mT is the amount that has an effect on the flow and not only did not suppressed the convective motion but also had negative impact on the fluid flow. Figure 11-a-b show that the speed fluctuation in both radial and circumferential direction is about two thousands times faster than that of the axial direction Fig 11-c. As figure 12 presents the contours of silicon distribution which are no longer parallel to the growth interface and start having a non-linear behavior which indicates an undesirable movement in the solvent region as a result of magnetic field.

6.2.4 Applied 15mT Magnetic Force with 2 rpm

In order to further investigate and determine whether more rotation can rectify the problem which occurred in the last case or can intensify the convective motion in the solute, a two rotation per minute was applied. Figure 13 illustrates the silicon distribution contours in the vertical cross section plane passing through the "z" axis of the model which runs through the origin of the model located in the center of the growth interface.

Results presented in Figure 12 reveal that the concentration of silicon is completely destabilized and a convection in the flow appears as a result of the application of Ω = 2 rpm along with the B=15mT and clearly can be seen that the uniform contour pattern are changing to a non uniform pattern in another word the convective motion appears to begin which is not desirable for crystal growth process.

Figure 13 shows that the effects of the g-jitter under the influence of the rotating

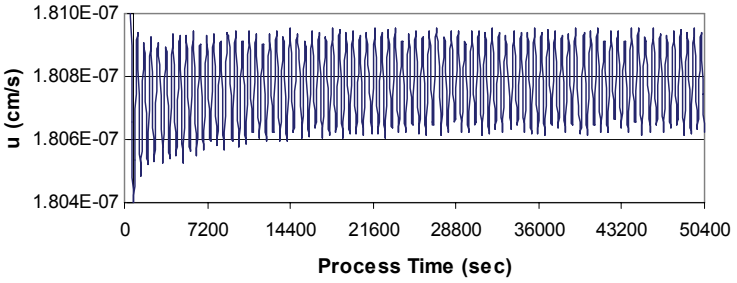

(a) Radial direction

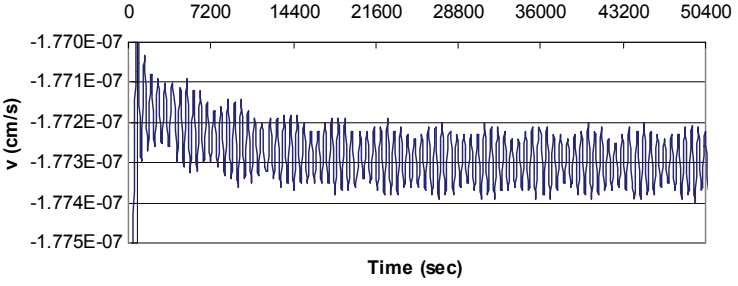

(b) Circumferential direction

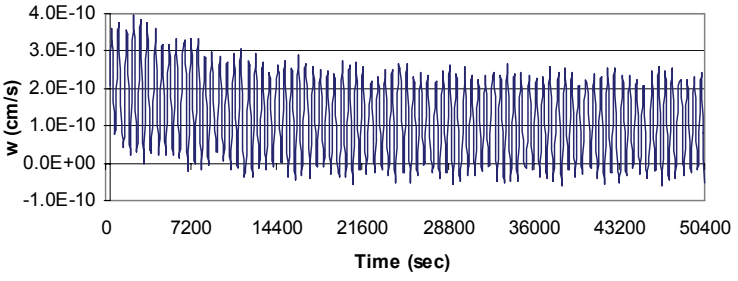

(c) Axial direction

Figure 11: Velocity Plots with B=15mT and Ω = 1/12 rpm for the first 14 hours of process

magnetic field in three different directions and clearly can be seen that the magnitude of velocity in each direction has been intensified. This increase is about thirty five times in the radial direction (Fig. 14-a) and about two hundred times in the axial direction (Fig. 14-c), however, as for the circumferential direction (Fig. 14-b), the velocity became eight times slower with this additional rotation.

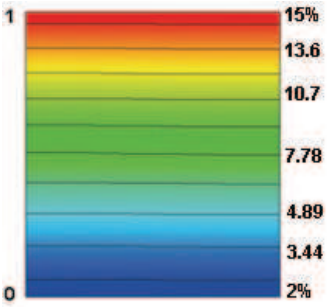

Figure 12: Silicon distribution contour with B=15mT and Ω = 1/12 rpm

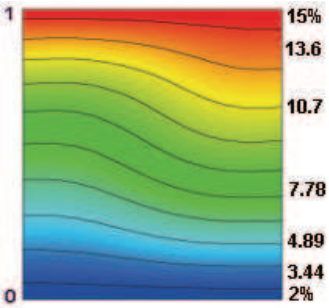

Figure 13: Silicon distribution contour with B=15mTand Ω = 2 rpm

6.2.5 Evaluating the frequencies

It was found that the external vibration's frequencies collected from FOTON as presented in appendix "B" are being damped in the solvent region and found to be less than 1.6 x 10^{-3} Hz in all three cases, this can be translated for each axis compared to that of the FOTON's as follow;

- For "r" axis about 0.3 percent reduction
- For "ϕ" axis about 37 percent reduction
- For "z" axis about 61 percent reduction

7 Conclusion

The effects of the low frequency g-jitter reported by the orbiter FOTON-M2, on the growth of bulk single crystal of $Ge_{0.98}$ $Si_{0.02}$ in the presence of rotating magnetic

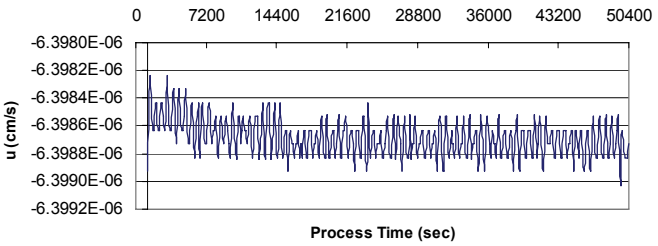

(a) Radial direction

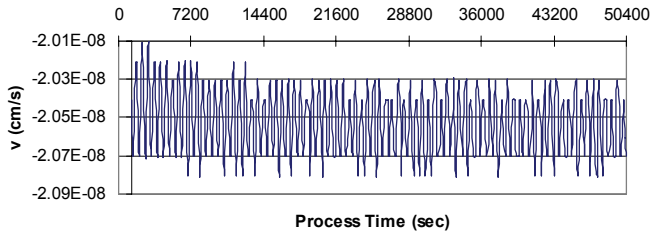

(b) Circumferential direction

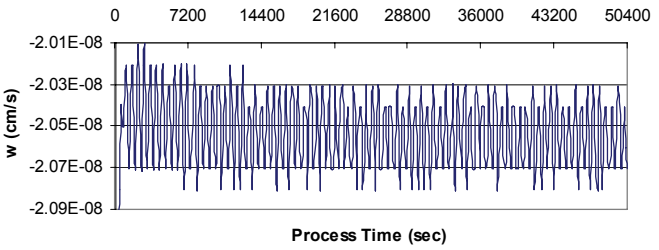

(c) Axial direction

Figure 14: Velocity Plots with B=15mT and Ω = 2 rpm for the first 14 hours of process

field were studied. The results which obtained by modeling and simulating the process indicate that the low frequency g-jitter has no significant effect on silicon distribution in solute and unlike the positive effect and promising result achieved in the authors former study in terrestrial environment, the rotating magnetic field has no positive impact on the solvent region of this model of TSM when the process is being conducted in microgravity and the frequencies are as low as collected by FOTON.

Acknowledgement: The authors would like to thank Natural Science and Engineering Council of Canada (NSERC) for their financial support on this study.

References

Ghaddar, C. K.; Lee, C. K.; Motakef, S.; Gillies, D. C. (1999): Numerical Simulation of THM growth of CdTe in presence of Rotating Magnetic Field (RMF), *Journal of Crystal Growth*, Vol. 250, pp. 99-111.

Gelfgat, M. (1995): MHD Flows in a Rotating Magnetic Field (a review), *Magnetohydrodunamics*, vol.31, no. 1-2, pp. 188-200.

IUPAC (1982): *International Union of Pure and Applied Chemistry Report, Internet edition on Semiconductors*, 54, 1533.

Labrie, D.; George, A. E.; Jamieson, M.; Obruchkov, S.; Healey, J. P.; Paton, B. E.; Saghir, M. Z. (2005): Homogeneity of Ge_x Si_{1-x}alloys (x <=0.30) govern by the traveling solvent method, International Jornal of Materials and product Technology, Vol. 22, No. 1/2/3, pp. 105-121.

Lehoczky, S.; Szofran, F. R.; Gillies, D. C. (1994): *Growth of solid solution single crystals" Second United States Microgravity Payload. Six Month Sciences Report.* NASA MSC.

Li, B. Q. (1996): G-jitter induced free convection in a transverse magnetic field. *Int'l. Jour. Heat/mass transfer*, Vol. 39, No. 14, pp.2853-2860.

Muller, G.; Baumgartl, J. (1996): The use magnetic fields for damping the action of gravity fluctuations (g-jitter) during crystal growth under microgravity. *Journal of Crystal Growth*, 169, pp. 582-586.

Yan, Y.; Pan, S.; Jules, K.; Saghir, M.Z. (2007): *Vibrational effect on thermal diffusion under different microgravity environment.* Z-Tech Publishing, Bremen Microgravity sci. technol. XIX-2.

Yasuda, H., Minakuchi, H., Okano, Y. Dost, S. (2004): Meeting Abstracts, pp. 72.

Yeckel, A.; Derby, J. J. (2004): Dynamics of 3-dimensional convection in microgravity crystal growth: g-jitter with steady magnetic fields. *Journal of Crystal Growth*, 263, pp. 40-52.

Appendix A

The uniform heating profile, below, is plotted based on the polynomial obtained from the Dalhousie University which is an experimented result applied on the model.

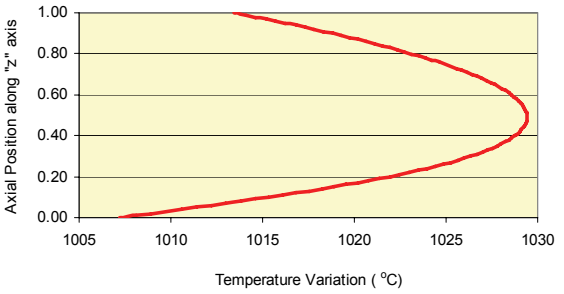

This profile reveals the temperature at dissolution interface, at top, is 1016.1 °C and at the bottom, growth interface is 1007.2 °C and the maximum is 1029.4 °C.

Appendix B

Table 2: Amplitudes and frequencies on board of FOTON-M2

Axis	j	a_0 $(10^{-6}m/s^2)$	a_j $(10^{-6}m/s^2)$	b_j $(10^{-6}m/s^2)$	f_j $(10^{-3}Hz)$
X	1	-3.6615	-24.896	30.786	1.64521
Y	1	-116.65	1.5392	0.42332	1.15756
	2	——	3.3976	-7.5033	2.51535
	3	——	4.1744	1.4193	1.87293
	4	——	-4.7073	-2.655	2.23785
	5	——	-0.96563	-1.4247	3.2815
Z	1	16.508	5.5583	2.8422	1.64353
	2	——	-0.45562	-0.7039	1.87083
	3	——	-1.5791	-0.09407	2.07368
	4	——	-2.8356	1.0229	3.2904
	5	——	-0.91597	-0.27967	4.14957

Appendix C

$$R=\frac{r}{L},\quad U=\frac{u}{u_0},\quad V=\frac{v}{u_0},\quad W=\frac{w}{u_0},\quad Z=\frac{z}{L},\quad \theta=\frac{T-T_0}{\Delta T},\quad C=\frac{c-c_0}{\Delta c},$$

$$P=\frac{pL}{\mu u_0},\quad B^*=\frac{B}{|B_0|},\quad \omega^*=\frac{\omega L}{u_0},\quad F=\frac{fL}{u_0}\tau=\frac{tu_0}{L}$$